On the Patterns of Wind-Power Input to the Ocean Circulation

FABIEN ROQUET AND CARL WUNSCH

Department of Earth, Atmosphere and Planetary Science, Massachusetts Institute of Technology, Cambridge, Massachusetts

GURVAN MADEC

Laboratoire d'Océanographie Dynamique et de Climatologie, Paris, France

(Manuscript received 1 February 2011, in final form 12 July 2011)

ABSTRACT

Pathways of wind-power input into the ocean general circulation are analyzed using Ekman theory. Direct rates of wind work can be calculated through the wind stress acting on the surface geostrophic flow. However, because that energy is transported laterally in the Ekman layer, the injection into the geostrophic interior is actually controlled by Ekman pumping, with a pattern determined by the wind curl rather than the wind itself. Regions of power injection into the geostrophic interior are thus generally shifted poleward compared to regions of direct wind-power input, most notably in the Southern Ocean, where on average energy enters the interior 10° south of the Antarctic Circumpolar Current core. An interpretation of the wind-power input to the interior is proposed, expressed as a downward flux of pressure work. This energy flux is a measure of the work done by the Ekman pumping against the surface elevation pressure, helping to maintain the observed anomaly of sea surface height relative to the global-mean sea level.

1. Introduction

The wind stress, along with the secondary input from tides, provides the main source of mechanical energy compensating the continuous loss to friction (Wunsch and Ferrari 2004). Knowledge of the distribution and fate of the wind stress power input to the ocean is essential for the understanding of the ocean circulation and its variability. Among the wide range of ocean movements induced by the wind forcing, the large-scale ocean general circulation is of special interest. This paper aims at better understanding where and how wind powers the ocean general circulation.

Several global estimates of power input to the ocean general circulation have been made, ranging between about 0.75 and 1 TW (Wunsch 1998; Huang et al. 2006; von Storch et al. 2007; Hughes and Wilson 2008; Scott and Xu 2009). Other sources of wind-power input are comparatively large, such as the power input to the ageostrophic circulation (about 3 TW; Wang and Huang 2004a) or the input to surface gravity waves (60+ TW; Wang and Huang 2004b), but they are not directly related to the interior flow.

Three methods for determining the local rate of wind-power input to the ocean general circulation have been proposed in the literature: 1) the direct rate of work on the geostrophic circulation (Stern 1975); 2) the rate at which the Ekman transport crosses the surface pressure gradient (Fofonoff 1981); and 3) the rate at which Ekman pumping generates potential energy in a stratified fluid (Gill et al. 1974). Only the first form has been used to make global estimates. That these three views must be equivalent was known to these authors, but exactly how that equivalence comes about is not obvious. Note, for example, that the two first forms depend on the wind stress but the third depends on the wind stress curl, and thus one expects their spatial patterns to be different.

In this paper, two alternative expressions for the rate of wind-power input into the geostrophic interior are derived. To illustrate the concepts developed later, Fig. 1 displays estimates of these two expressions for the Southern Ocean, which were made by methods to be described later. The first maps corresponds to the direct rate of wind-power input to the geostrophic circulation (Stern and Fofonoff views), whereas the second map (somewhat

Corresponding author address: Fabien Roquet, Department of Earth, Atmosphere and Planetary Science, Massachusetts Institute of Technology, Cambridge, MA 02139.
E-mail: roquet@mit.edu

DOI: 10.1175/JPO-D-11-024.1

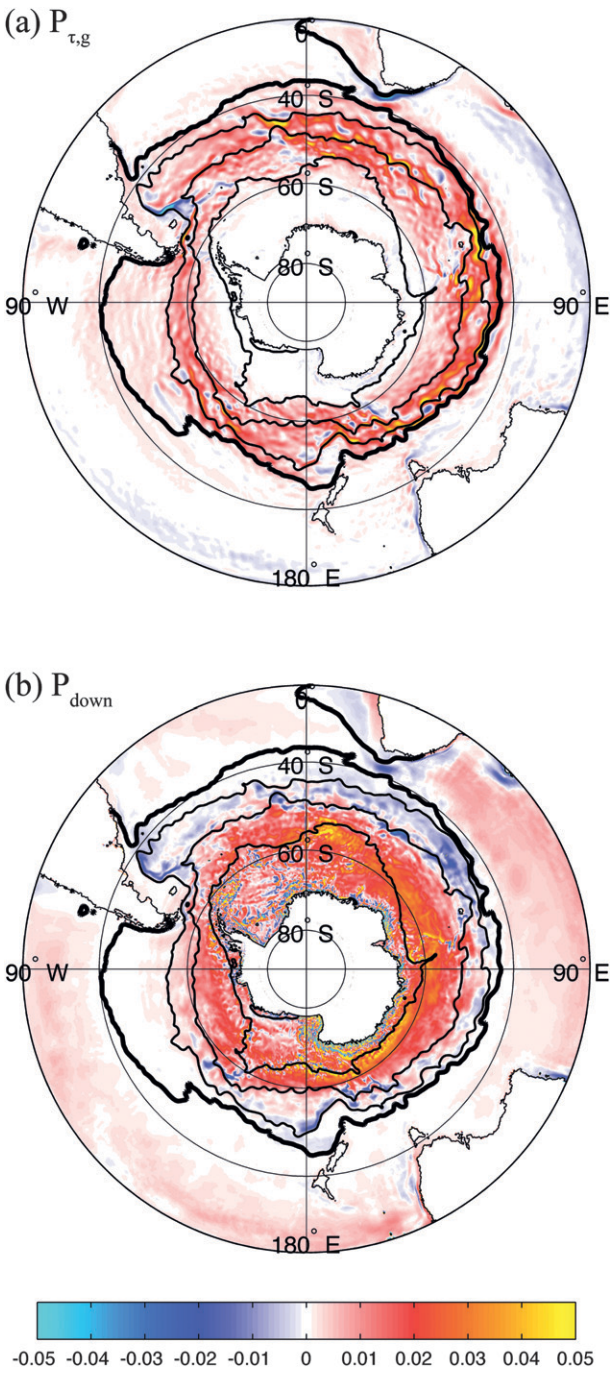

FIG. 1. Maps of (a) $P_{\tau,g} = \langle \tau_0 \cdot \mathbf{u}_g \rangle$ and (b) $P_{\text{down}} = \langle -\rho_0 g \eta w_{\text{Ek}} \rangle$ (W m^{-2}), where $\langle \cdot \rangle$ is a temporal average estimated from daily outputs of the SOSE (Mazloff et al. 2010). Contours of global-mean sea level (thick line), and of northern, middle, and southern ACC boundaries (thin lines) are superimposed. These two maps represent alternative ways of representing the wind-power input to the geostrophic circulation.

closer to the Gill view) represents the input of pressure work injected into the interior ocean. Although the representations have different spatial patterns, they are equivalent in the sense that their integrals over the global ocean are strictly identical, as will be shown.

After presenting a theoretical description of wind-related energy pathways and their physical significance, realistic estimates will be proposed for the global ocean. A more detailed examination will then be undertaken of the Southern Ocean, which has the most conspicuous importance to the energetics. Because the physics employed here are elementary—geostrophic flows and Ekman layers—the chief goal is insight into energy pathways as a means to better understanding rather than any new general circulation properties.

2. The rate of wind work on the interior

a. Ekman pumping

As has been clear since the work of Stommel (1957), Ekman pumping of the geostrophic interior represents a major control on the general circulation. To establish a notation, consider, as is done classically, a steady state with a balance between the Coriolis force, the horizontal pressure gradient, and the applied wind stress forcing in a Boussinesq approximation. The flow is split into geostrophic and ageostrophic components. Wind stress generates an ageostrophic Ekman layer, which is typically assumed shallower than about 100 m and is defined as sufficiently deep to neglect the ageostrophic circulation at its bottom.

Net Ekman transport (i.e., the ageostrophic lateral volume transport) is

$$\mathbf{U}_{\text{Ek}} \equiv \int_{\text{Ek}} \mathbf{u}_a \, dz = -\frac{1}{\rho_0 f} \mathbf{k} \times \boldsymbol{\tau}_0, \tag{1}$$

where ρ_0 is a density of reference, f is the Coriolis parameter, $\mathbf{k}$ is the vertical unit vector, and $\boldsymbol{\tau}_0$ is the surface wind stress. In the following, $\mathbf{u}$ and w are the horizontal and vertical velocities, respectively, the subscripts a and g refer to ageostrophic and geostrophic components, respectively. Continuity of flow implies a vertical velocity component at the sea surface,

$$w_a(z = 0) = -\nabla_h \cdot \mathbf{U}_{\text{Ek}}. \tag{2}$$

To satisfy the surface boundary condition of no-normal flow, this surface ageostrophic vertical velocity must be balanced by an equal and opposite surface geostrophic vertical flow, called vertical Ekman velocity, which drives the ocean geostrophic interior,

$$w_{\mathrm{Ek}} \equiv w_g(z = 0) = \nabla_h \cdot \mathbf{U}_{\mathrm{Ek}} = \nabla \times \left(\frac{\boldsymbol{\tau}_0}{\rho_0 f}\right). \quad (3)$$

The simple dynamics of Ekman pumping breaks down near coasts, as the presence of sidewalls is increasingly felt by the flow. The wind stress vanishes at the coastline, which implies a singularity of its curl. In reality, higher-order physics applies in coastal boundary layers (e.g., Pedlosky 1968). To account for this higher-order physics in a simple way, we will assume that the Ekman transport, along with the wind stress injected to the ocean fluid, decays continuously to zero at the coastline. This assumption permits extension of the third definition of the vertical Ekman velocity to the regions near the boundaries, implying that the global vertical transport induced by Ekman pumping is zero (using the divergence theorem),

$$\int\int_{\mathrm{ocean}} w_{\mathrm{Ek}}\, dS = 0. \quad (4)$$

In the existing literature, vertical Ekman velocity is often described as induced directly at the bottom of the Ekman layer (e.g., Stern 1975). This view, derived from a boundary layer model with infinitesimal thickness, constitutes an excellent approximation but is never exactly true, even for a constant-density Ekman layer. Here, the vertical Ekman velocity is directly defined at the surface.

b. Wind work on the pressure field

The direct rate of wind work on the surface geostrophic flow is

$$P_{\tau,g} \equiv \boldsymbol{\tau}_0 \cdot \mathbf{u}_g(z = 0) = \boldsymbol{\tau}_0 \cdot \left(\frac{1}{f\rho_0}\mathbf{k} \times \nabla_h p_0\right), \quad (5)$$

where p_0 is the pressure evaluated at $z = 0$. Rewriting (5) using (1),

$$P_{\tau,g} = \mathbf{U}_{\mathrm{Ek}} \cdot \nabla_h p_0, \quad (6)$$

showing that the rate of wind work on the surface geostrophic flow equals the power produced by the Ekman circulation crossing the surface pressure gradient (Fofonoff 1981).

The power input can then be further rewritten,

$$\begin{aligned} P_{\tau,g} &= -p_0 \nabla_h \cdot \mathbf{U}_{\mathrm{Ek}} + \nabla_h \cdot (p_0 \mathbf{U}_{\mathrm{Ek}}) \\ &= -p_0 w_{\mathrm{Ek}} + \nabla_h \cdot (p_0 \mathbf{U}_{\mathrm{Ek}}), \end{aligned}$$

or, writing the hydrostatic pressure at $z = 0$ as a function of the sea surface height (SSH) $p_0 = \rho_0 g \eta$,

$$P_{\tau,g} = P_{\mathrm{down}} + P_{\mathrm{lat}}, \quad (7)$$

where

$$P_{\tau,g} = \rho_o g \mathbf{U}_{\mathrm{Ek}} \cdot \nabla_h \eta, \quad (8)$$

$$P_{\mathrm{down}} = -\rho_o g \eta w_{\mathrm{Ek}}, \quad \text{and} \quad (9)$$

$$P_{\mathrm{lat}} = \nabla_h \cdot (\rho_o g \eta \mathbf{U}_{\mathrm{Ek}}). \quad (10)$$

The term $P_{\tau,g}$ is equal to the sum of a downward flux of pressure work P_{down} with a lateral divergence term P_{lat} defined as the horizontal divergence of a (depth integrated) lateral flux of pressure work,

$$\phi_{\mathrm{lat}} \equiv \rho_0 g \eta \mathbf{U}_{\mathrm{Ek}}. \quad (11)$$

This decomposition shows that only a part of the local power input is injected locally in the interior as a flux of pressure work, with the remaining part being first transported laterally to be injected elsewhere. The lateral flux of pressure work thus plays a major role in redistributing the energy inside the Ekman layer, before its input to the interior.

Relation (7) applies independently of the level used to reference the sea surface height. Indeed, $P_{\tau,g}$ is independent of this level, and any change in level height induces additional terms in P_{down} and P_{lat} that are equal and opposite. Mean sea level is nonetheless the most natural choice. Indeed, because the spatial average of the vertical Ekman velocity has been set to zero [see Eq. (4)], only the sea surface height anomaly relative to the global-mean sea level is involved in P_{down},

$$\overline{P_{\mathrm{down}}} = -\rho_0 g \overline{\eta}\, \overline{w_{\mathrm{Ek}}} - \rho_0 g \overline{\eta' w'_{\mathrm{Ek}}} = -\rho_0 g \overline{\eta' w_{\mathrm{Ek}}}$$

where $\bar{\cdot}$ is the spatial average and $\cdot'$ is the anomaly relative to the spatial average. To simplify notation, the prime will be dropped hereafter, meaning that η corresponds to the horizontal anomaly of sea surface height relative to global-mean sea level in the following.

c. Physical interpretation

When integrated over the global ocean, the lateral divergence term vanishes because the lateral flux of pressure work itself vanishes at the boundaries, from the assumption of no Ekman transport across boundaries. Thus, the total wind stress power input to the geostrophic circulation is equal to the total downward flux of pressure work,

$$\int\int_{\mathrm{ocean}} P_{\tau,g}\, dS = \int\int_{\mathrm{ocean}} P_{\mathrm{down}}\, dS. \quad (12)$$

The local inputs $P_{\tau,g}$ and P_{down} thus provide two equivalent but different views of how the wind-related power enters the geostrophic interior by Ekman pumping. Equation (8) shows that $P_{\tau,g}$ is the rate of work done by the Ekman circulation to maintain a local slope of the sea surface. In contrast, P_{down} measures the rate of work done by Ekman pumping to maintain the local anomaly of sea surface height relative to global-mean sea level. This work is positive if the Ekman pumping (expressed as $-\rho_0 g w_{\text{Ek}}$, a vertical pressure per unit time) has the same sign as the observed sea surface anomaly.

To gain further insight into the physical significance of these flux terms, a balance of kinetic energy in a constant-density Ekman layer model is presented in appendix A. In that model, only the wind stress work on the geostrophic circulation powers the hydrostatic pressure field [Eq. (A6)], whereas the work on the wind-induced ageostrophic circulation is entirely dissipated in the Ekman layer, which is used to sustain the Ekman spiral.

The direct rate of power input to the geostrophic circulation $P_{\tau,g}$ is transformed into fluxes of pressure work (either lateral or vertical) or converted into potential energy inside the Ekman layer [Eq. (A5)]. A simple relation between P_{down} and the downward flux of pressure work at the bottom of the Ekman layer is finally obtained [Eq. (A7)], showing that P_{down} accounts for all energy terms associated with the geostrophic circulation, including fluxes and conversions inside the Ekman layer, as well as the fluxes of pressure work entering below the Ekman layer.

The term P_{down} thus provides an expression for the power input to the geostrophic interior, directly expressed from the surface. In contrast to the downward flux of pressure work expressed at the bottom of the Ekman layer, P_{down} is independent of the choice of Ekman depth and directly includes the geostrophic energy fluxes flowing into both the Ekman layer and the interior. This property is appealing because the vertical scale of the geostrophic circulation is independent of the Ekman layer depth, being far greater.

Although not considered in appendix A, steric effects on the pressure are in reality not everywhere negligible in the Ekman layer. They make the global input of pressure work at the Ekman depth slightly less than the surface input (von Storch et al. 2007), because of a net conversion of kinetic energy into potential energy lying inside the surface layer. Considering pressure work inputs directly at the surface and then allows a clearer separation between wind-induced surface input and subsequent internal fluxes and conversions of energy, which lie both in the Ekman layer and below.

Global estimates of surface wind-work inputs in the real ocean will now be presented, based on the relation (7) only. No attempt will be made to estimate the internal pathways of energy below the Ekman layer in this paper, with that analysis being postponed to a future publication.

3. Global estimate

a. Data and method

To estimate the rate of wind work requires estimates of the wind stress and the surface oceanic geostrophic flow fields. For the global estimate, only the time-mean contribution to wind-power input is considered: that is, the spatial correlation of the time means. Time-varying power inputs will be discussed later through the diagnostic of an eddy-permitting Southern Ocean state estimate (SOSE; Mazloff et al. 2010). For now, simply note that, because the spatial correlations between oceanic and atmospheric variability are generally small, the time-dependent terms are known to be relatively small but not negligible (e.g., Hughes and Wilson 2008).

The time-mean surface flow of reference is estimated using the mean dynamic topography of the Ocean Comprehensible Atlas (OCCA; Forget 2010) (see Fig. 2a). OCCA is a global ocean circulation estimate in the 2004–06 period from the Estimating the Circulation and Climate of the Oceans (ECCO) family of estimates. It is based on the ECCO configuration of the Massachusetts Institute of Technology general circulation model (MITgcm; Marshall et al. 1997) with a 1° horizontal resolution and constrained by weighted least squares as described by Forget (2010). A comparison with the combined mean dynamic topography of Rio and Hernandez (2004, hereafter RH04) shows only relatively small and localized differences, with a global RMS difference of 7 cm out of a total range of about 2 m. The uncertainty of the global-mean sea surface height product is likely greater in reality, because both compilations are based on similar datasets with common biases. It must also be kept in mind that OCCA is a 3-yr-long average, not a climatology.

The reference wind stress product (NCEPbulk) is derived from the National Centers for Environmental Prediction—National Center for Atmospheric Research (NCEP–NCAR) reanalysis surface wind fields (Kalnay et al. 1996) using the bulk formulas of Large and Yeager (2004),

$$\boldsymbol{\tau}_0 = \rho_{\text{air}} C_{\text{drag}} |\mathbf{u}_{\text{air}}^{10\text{m}} - \mathbf{u}| (\mathbf{u}_{\text{air}}^{10\text{m}} - \mathbf{u}), \qquad (13)$$

where ρ_{air} is the air density, C_{drag} is the drag coefficient, $\mathbf{u}_{\text{air}}^{10\text{m}}$ is the wind speed at 10 m, and $\mathbf{u}$ is the surface ocean velocity. Although ocean currents are generally small compared to wind speed, their inclusion in the stress calculation introduces a systematic correlation between

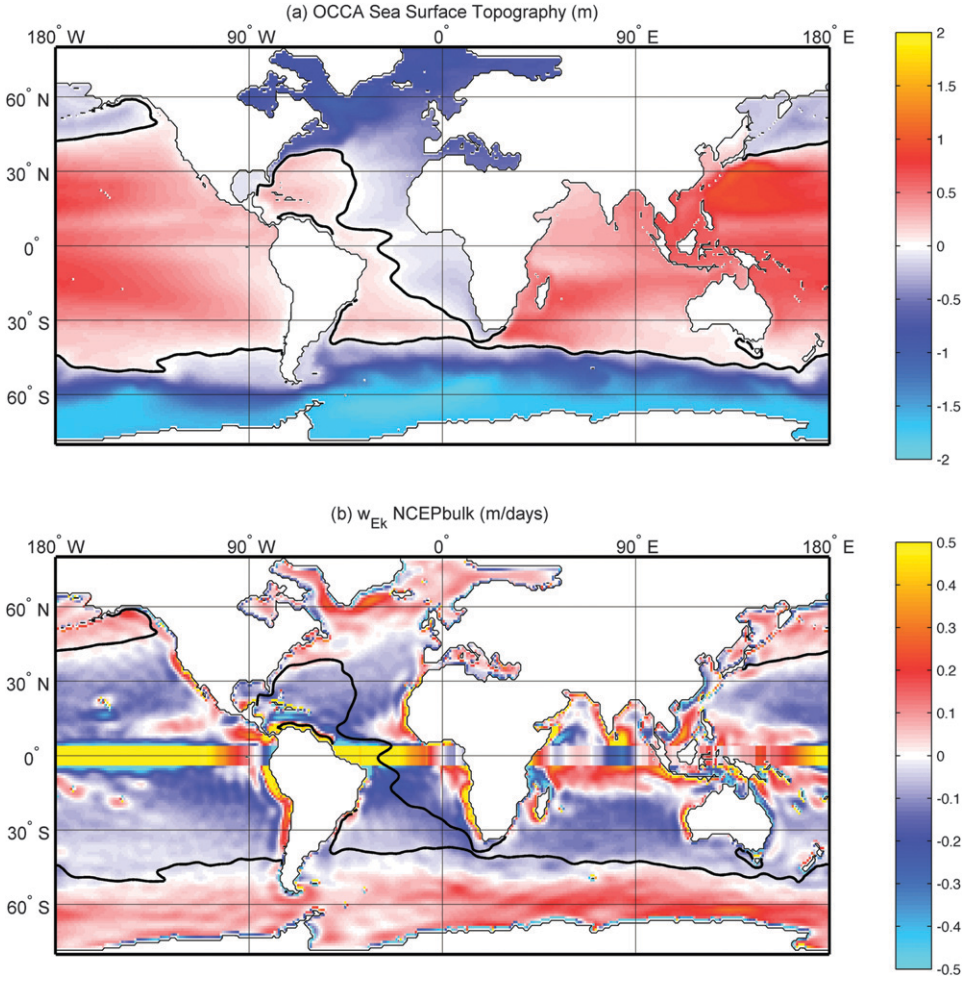

FIG. 2. (a) Mean sea surface topography derived from OCCA (Forget 2010). The color scale is centered on the global-mean SSH (thick black line contour). (b) Mean vertical Ekman velocity w_{Ek} (m day^{-1}), defined as the wind-induced surface geostrophic vertical velocity. The equatorial values are based on the meridional divergence of Ekman transport between 3°S and 3°N, transporting up 97 Sv. The global-mean sea level contour is repeated (thick black line) to highlight the spatial correlations between the two fields.

wind stress and ocean velocity leading to a 20%–35% reduction of the wind-power input (Duhaut and Straub 2006; Hughes and Wilson 2008). This so-called relative wind effect is here accounted for by using OCCA surface daily currents.

A map of the vertical Ekman velocity w_{Ek} calculated from NCEPbulk, is presented in Fig. 2b, showing a strong zonality related to the large-scale structure of the zonal wind stress. In both hemispheres, a change of sign of the Ekman pumping is observed near 40° latitude, separating the subpolar (positive) and subtropical (negative) areas. When integrated spatially, Ekman divergence upwells about 30 Sv (1 Sv $\equiv 10^6$ m^3 s^{-1}) in the Southern Ocean and 10 Sv in the northern Atlantic and Pacific. Subtropical areas are downwelling regions, transporting downward about 90 Sv in the Southern Hemisphere and about 45 Sv in the Northern Hemisphere. A large fraction of the subtropical near-equator downwelling is compensated by a strong upwelling induced in the equatorial band (95 Sv in the 3°S–3°N band). The global-mean sea level contour extracted from OCCA (Fig. 2a) is superimposed on the map of w_{Ek}. In many places, the global-mean sea level contour follows closely the transition zone where Ekman pumping changes sign. This spatial correlation between the two fields is in fact not really surprising for a primarily wind-driven ocean circulation, because Ekman convergence should cause higher sea levels on average and vice versa.

Fluxes of wind power are diagnosed using the set of Eqs. (7)–(10), discretized on the OCCA C grid (see Forget

TABLE 1. Area-integrated power inputs (GW) associated with Ekman pumping. Only the time-mean contribution is calculated. The products used in each case are listed: OCCA (Forget 2010) and RH04 for SSH products and NCEPbulk (based on a bulk calculation using NCEP winds), SCOW (Risien and Chelton 2008), NCEP wind stress, and OCCA-adjusted wind stress for wind stress products. More details can be found in the core text and in appendix C.

SSH Wind stress	OCCA NCEPbulk	OCCA SCOW	OCCA NCEP	RH04 NCEPbulk	RH04 SCOW	RH04 NCEP	OCCA OCCA
Global input	655	700	809	671	720	840	988
North of 40°N	33	31	43	37	36	47	55
40°S–40°N	176	221	189	175	223	198	300
South of 40°S	446	448	578	458	461	594	633
Equator 3°S–3°N	4	11	4	0	6	−2	14
Upwelling (Sv)	97	131	115	97	131	115	115
Pressure work input	−311	−440	−360	−298	−422	−344	−340

2010). The methodology used to calculate wind-work terms in the equatorial band is given in appendix B. The width of the equatorial band (3°S–3°N) considered for calculation is somewhat arbitrary but is a common choice in the literature, and the results here are not sensitive to it. Discretization error, estimated as the residual of the three power flux terms in the relation (7), is negligible everywhere. The global balance (12), between wind stress work and pressure work flux to the interior, is consistent to high accuracy, with only 1 GW of difference out of 655 GW of total input.

NCEPbulk was chosen as the reference because it is based on a standard wind product with a global coverage (contrary to satellite-based products) and accounts for the relative wind effects in a simple and straightforward way. It was decided not to use the OCCA-adjusted wind stress field as the reference, because the OCCA wind adjustments are large and induce a complicated pattern of small-scale anomalies not observed in other wind products. It is to be noted, however, that the large-scale patterns of wind-power input obtained with the OCCA-adjusted winds remain essentially the same as for the other tested wind products.

To further test the reference choice and to obtain at least a rough idea of the uncertainties in power input estimates, they are compared with results obtained from a number of alternative estimates of both fields (see appendix C). Table 1 presents area-integrated power input for these estimates. Total wind stress power inputs range between about 660 and 990 GW, depending mostly on the choice of wind stress product. About two-thirds of the wind-power input occurs in the Southern Ocean, with 20%–30% coming from subtropical areas, leaving a very minor input for the boreal subpolar area (less than 10%). A summary of these product comparisons would be that results presented below are qualitatively insensitive to alternative choices, although the uncertainty of the magnitude of power fluxes remains large (up to 50%).

b. Spatial patterns

Power input maps derived from the OCCA–NCEP bulk diagnostic are shown in Fig. 3, including $P_{\tau,g}$, P_{down}, and P_{lat}. Lateral flux vectors $\boldsymbol{\phi}_{\mathrm{lat}}$ are superimposed on the map of their horizontal divergence. For completeness, zonal integrals of wind-induced power fluxes and their northward accumulation are shown in Fig. 4.

In accord with previous analyses, the largest input to the geostrophic circulation is located along the Antarctic Circumpolar Current (ACC), with secondary inputs along western boundary currents and around the equator. Wind stress only rarely works against the geostrophic currents. In general, however, the spatial pattern of downward flux into the ocean interior P_{down} is substantially different from the direct rate of wind input. This difference arises from the lateral fluxes of pressure work, mostly directed poleward (see arrows in Figs. 3c, 4b), and is particularly clear in the Southern Ocean, where the large inputs of wind power are shifted by about 10° southward before being injected into the interior. A more detailed pattern of energy injection in the Southern Ocean will be discussed later.

Except in the Pacific equatorial band, and along a few coastal regions, the downward input of pressure work is generally positive, resulting from the spatial correlation between vertical Ekman velocity and sea surface topography noted earlier (see Fig. 2). The Pacific equatorial band is a major sink of pressure work (−310 GW), because of the large equatorial upwelling (about 100 Sv transported in the 3°S–3°N latitude band) in a region of positive sea surface anomaly. The net input of wind work to the geostrophic circulation there is nevertheless small, ranging from 0 to 10 GW (see appendix B for the method of calculation) because of a large lateral fluxes on both sides of the equatorial Pacific, which compensates most of the downward flux. The sink of downward pressure work must in practice be balanced by a convergence of pressure work in the interior, which is probably related

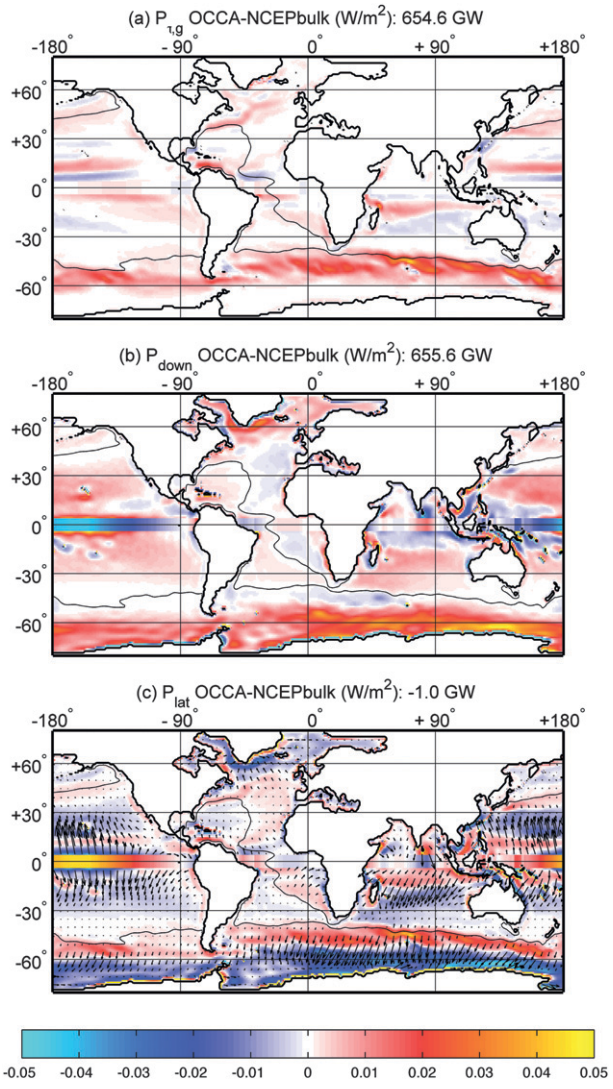

FIG. 3. Time-mean contribution of energy input rates estimated using the OCCA–NCEPbulk combination described in the text: (a) $P_{\tau,g}$, (b) P_{down}, and (c) P_{lat} given in W m^{-2}. The lateral flux vector ϕ_{lat} is superimposed on its divergence map. The OCCA global-mean sea level contour (see Fig. 2a) is also shown. By definition, P_{down} and ϕ_{lat} are zero along this contour. Global integrals of $P_{\tau,g}$ and P_{down} should be strictly equal [see Eq. (12)]; however, a negligible −1-GW difference is found because of discretization errors.

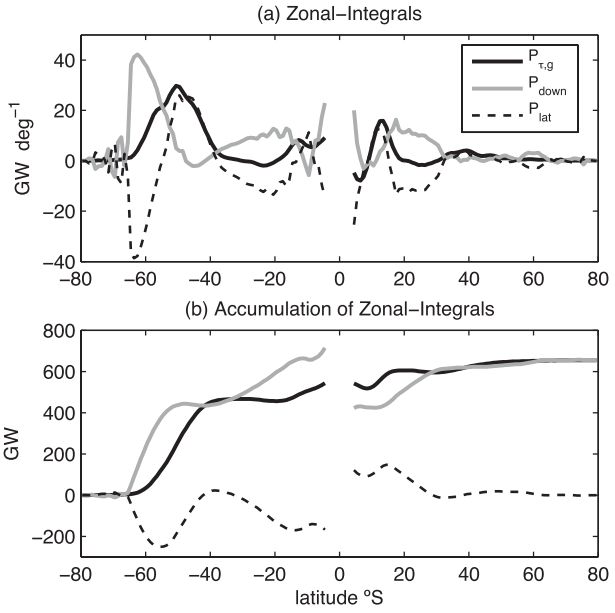

FIG. 4. (a) Zonal integrals of wind stress work components using the OCCA–NCEPbulk combination. (b) Northward accumulation of the zonal integrals. The accumulation of the lateral divergence term corresponds to the total flux of lateral power crossing each parallel, showing that in general lateral fluxes are directed poleward.

to the equatorial convergence of geostrophic flow and to the eastward equatorial undercurrent.

In comparison with the Pacific, the Atlantic basin presents a somewhat reversed pattern of power injection, with low fluxes in the subtropical areas and larger values in the northern subpolar area. Unlike other regions, the mean sea level contour does not completely follow the transition zone where the vertical Ekman velocity changes sign in the Northern Hemisphere, diverging importantly east of the mid-Atlantic ridge and crossing the entire Atlantic basin to the southern tip of Africa. As a consequence, the downward and lateral fluxes of pressure work are everywhere small in the subtropical and tropical areas of the Atlantic basin. This region shows the largest divergence of the spatial patterns of Ekman pumping and the sea surface topography, which may indicate a larger role of the interior circulation in shaping the sea surface topography there.

The spatial pattern of wind-induced energy fluxes is very robust to the choice of wind stress or sea surface height products, because it is strongly constrained by stable features of the atmospheric and oceanic circulation, such as the position of zero wind stress curl and the position of mean sea surface height. Calculated magnitudes of energy fluxes can vary by as much as 50% between different wind stress products (see Table 1 and appendix C), but the pattern itself is stable.

4. The Southern Ocean

The Southern Ocean is the major region of wind energy input into the ocean (Fig. 1), and it is worth exploring it in a bit more detail. Estimates are made using the SOSE described in detail by Mazloff et al. (2010). Like OCCA, SOSE is part of the ECCO family of ocean circulation estimates. It is an eddy-permitting configuration of the Southern Ocean (south of 25°S) with a

1/6° horizontal resolution integrated over the 2005–07 period and estimated using weighted least squares as described by Mazloff et al. (2010). SOSE yields a realistic-appearing model ACC with a mean transport of 150 ±5 Sv.

SOSE wind stress was again obtained by applying the bulk formulas of Large and Yeager (2004) to the NCEP wind field and the effect of ocean currents relative to atmospheric winds were taken into account. Wind field adjustments were made during the SOSE data-fitting process, although, unlike the OCCA results, the final estimated wind field does not differ qualitatively from the initial estimate (Mazloff et al. 2010) and the mean wind stress does not depart significantly from the NCEP-bulk values (relative change $< 5\%$).

Global-mean sea surface height cannot be derived directly from the regional SOSE estimate. The difference between global-mean and SOSE-domain mean sea surface height inferred from OCCA is −42 cm, which has thus been subtracted from the SOSE sea surface height anomaly. At the northern boundary, inflow–outflow conditions are directly derived from OCCA. Daily outputs of η and $\boldsymbol{\tau}_0$ from SOSE iteration 52 (M. Mazloff 2010, personal communication) are analyzed in the following.

The mean wind stress power input into the surface geostrophic circulation is shown in Fig. 1. Again the largest power input is found within the ACC belt, which combines strong westerly winds with strong eastward flow. To gain more insight into the spatial distribution, three selected isolines of mean sea surface height are used and designated as south, middle, and north ACC boundaries (taken as −160-, −95-, and −30-cm isolines), respectively. The south and north ACC boundaries enclose the Drake Passage, whereas the middle ACC one corresponds to the average SSH value between the two boundaries. These three boundaries approximately match the positions of the south ACC, Polar, and Subantarctic Fronts, respectively, as defined by Orsi et al. (1995). From south to north, the zones defined between these boundaries will be designated as subpolar, south ACC (S-ACC), north ACC (N-ACC), and subtropical zones. The global-mean sea surface height contour follows closely the definition of the subtropical front in the Southern Ocean.

Spatial integrals of power inputs and fluxes over each defined zone are given in Table 2. Total wind stress energy input to the geostrophic circulation is 430 ±100 GW in SOSE. This value is consistent with previous estimates, including the 480-GW estimate of Hughes and Wilson (2008). More than 75% of this energy is injected within the ACC zone, although it is only 31% of the domain area. High values of power input are especially found in the north ACC zone of the Indian Ocean sector, corresponding to the region of stronger westerlies.

TABLE 2. Area-integrated power inputs in SOSE (in GW). The direct wind input $P_{\tau,g}$, pressure work input P_{down}, and northward flux across the northern boundary $\boldsymbol{\phi}_{\text{lat},y}$ are given for each domains, along with their relative surface area. Domain boundaries are shown in Fig. 1.

	$P_{\tau,g}$	P_{down}	$\phi_{\text{lat},y}$	Area
Tot	426	492	−66	100%
Subtropical	81	98	−66	55%
ACC	333	263	−48	31%
N-ACC	192	−2	−48	15%
S-ACC	141	265	−242	16%
Subpolar	12	130	−118	14%

The spatial distribution of power input into the interior (Fig. 1) is radically different from wind stress input into geostrophic currents. Downward pressure work flux is positive everywhere south of the middle ACC boundary. It is zero on average over the north ACC zone. This large difference occurs because of the intense southward flux of pressure work in the Ekman layer. The flux is southward, although Ekman transport is northward, because the subpolar area is a low SSH region (negative anomaly), and Ekman transport drains water out of a low sea level region. Thus, the wind stress works to reinforce the observed SSH anomaly (positive work).

A 120-GW southward flux is found along the southern ACC boundary. This flux has been induced in the ACC area as a direct wind work but is injected to the interior in the subpolar area. One should not conclude that this flux would then power subpolar circulations rather than the ACC itself. Because the direct wind work is equivalent to the work done to produce a local sea surface slope [see relation (8)], the direct wind work over the ACC region effectively corresponds to a local acceleration of the ACC.

The southward flux across the south ACC boundary shows the fundamentally nonlocal nature of Ekman pumping. Slope production along the ACC induces a deficit of sea surface height not only over that current but also in the entire subpolar area. This deficit is powered by the downward pressure work resulting from a spatial correlation between sea surface height anomaly and Ekman pumping. Upwelling by Ekman pumping in the subpolar area thus participates significantly to the maintenance of the ACC circulation, illustrating the strong dynamical connections between adjacent circulations and more generally among all regions of the World Ocean.

5. Time-varying power inputs

The time-varying contribution to the wind-work input is generally small, because atmospheric and oceanic variability have very different spatial and temporal scales of variability, yielding little correlation between associated anomalies. It can however be locally important.

A stable pattern of strong positive and negative contributions occurs in the tropics (Wunsch 1998; von Storch et al. 2007; Hughes and Wilson 2008; Scott and Xu 2009). A positive input generally ranging between 30 and 60 GW is associated with this tropical pattern. Elsewhere, the time-varying contribution to the global input of wind work is highly sensitive to the inclusion of the relative wind effect (Duhaut and Straub 2006; Hughes and Wilson 2008; Scott and Xu 2009). Without the relative wind effect, the global input of wind work reflects mainly the tropical input. However, when the relative wind effect is taken into account, a negative contribution due to mesoscale activity nearly cancels the positive tropical contribution. Global estimates of time-varying wind-work input, including the relative wind effect, are thus generally very small, between 0 and 15 GW (Hughes and Wilson 2008; Scott and Xu 2009). A smaller positive contribution is generally found over continental margins, which could be related to coastal wave patterns or steric effects induced by coastal upwellings (Hughes and Wilson 2008).

The time-varying contribution is diagnosed in the eddy-permitting SOSE estimate, using daily outputs of wind stress and sea surface height (see Fig. 5). Overall, this contribution is very small, about 1 GW. The pattern of time-varying contributions to direct wind work and downward pressure flux are visually similar, although the former is somewhat noisier. Negative work is found in high eddy activity regions, superimposed on a pattern of weak positive work evenly distributed over most of the ACC area. The negative input is clearly associated with high eddy activity regions, where the relative wind effect is at maximum, in agreement with previous studies. It represents an input of -20 GW, which almost exactly cancels the smooth positive contribution mostly found along the ACC path and over continental margins. The fact that negative and positive time-varying contributions nearly cancel is likely fortuitous.

The positive contribution in the ACC area may be related to some of the seasonal variability introducing large-scale correlations between the wind strength and the ACC circulation. Existence of a large seasonal and interannual variability of the wind-work input has been described by Huang et al. (2006), who found a standard deviation of the input representing roughly 10% of the mean input. The positive contribution over continental margins is also consistent with the findings of Hughes and Wilson (2008). A longer time period of integration will be necessary to study the statistical robustness of these time-varying contributions, but it appears already at this stage that the time-varying power input is everywhere small, which justifies a posteriori the earlier study of global wind-work inputs based on the time-mean contribution only.

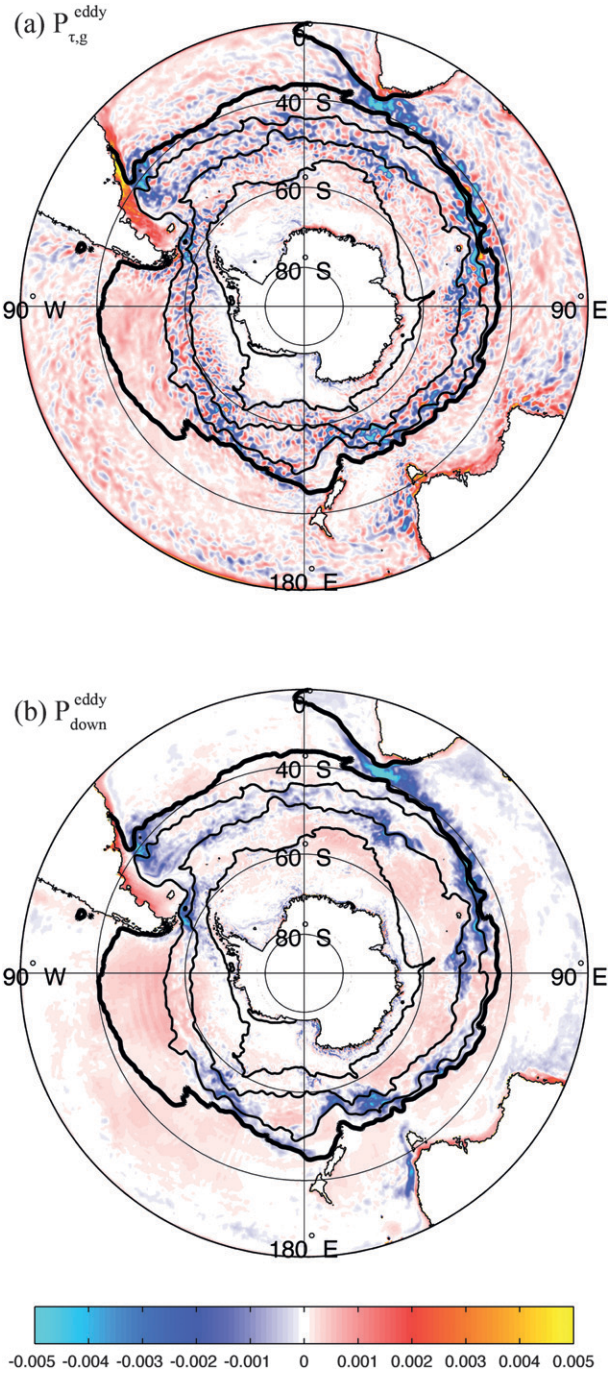

FIG. 5. As in Fig. 1, but for the time-varying contribution only. Note that the color scale used here is expanded 10 times compared to Fig. 1.

6. Discussion and conclusions

Two equivalent approaches exist for the calculation of the rate of wind work on the large-scale ocean circulation. Up to numerical inaccuracies, the net rates are identical when integrated over closed ocean basins. In contrast,

however, the spatial patterns of the time-average power inputs can be quite different. In particular, the regions of direct working on the circulation given by $\boldsymbol{\tau}_0 \cdot \mathbf{u}_g$ differs from the rate at which the energy is pumped through the Ekman layer into the interior circulation given by $-\rho_0 g \eta w_{\mathrm{Ek}}$. The energy flux is here reinterpreted as going first into the Ekman layer and then being transported laterally by the Ekman transport before being pumped into the interior circulation. Thus, the power available from the wind is commonly injected into the geostrophic circulation considerable distances from the region of direct wind work.

A number of comparisons of different sea surface height and wind stress products show a general stability of the spatial patterns of energy input and lateral transport, although magnitude of energy fluxes can vary importantly both locally and globally (up to 50%). This robustness of patterns comes from the stability of such features such as the position of the zero wind stress curl and the mean sea level contour constraining the sign and amplitude of energy fluxes.

Despite its importance as an energy source for the interior flow, the mean downward input of pressure work $-\rho_0 g \eta w_{\mathrm{Ek}}$ does not appear to have been previously mapped, perhaps because previous studies focused on its diagnostics at the bottom of the Ekman layer. A unique Ekman depth is generally impossible to define (e.g., von Storch et al. 2007), and the hypothesis of an infinitesimal Ekman layer thickness is difficult to defend for the real ocean, which renders its definition ambiguous. In our diagnostic, the depth of the Ekman layer does not appear because the flux of pressure work is considered directly at the surface. It is in fact not surprising that power inputs to the geostrophic circulation would not depend on the actual depth of the Ekman layer, because there is no direct relationship between the vertical scales of the Ekman layer and of the geostrophic circulation.

Referencing the sea surface height to global-mean sea level is a natural way to embed a principle of continuity in the diagnostic of energetics. It gives a local expression of the global connection between the circulation in the different basins: the action of the wind in a basin can act on the sea surface height in another basin. The downward input of pressure work is interpretable as the power generated locally by the Ekman pumping to maintain the sea surface height away from its level of equilibrium: that is, the global-mean sea level.

The direct input of wind power to the geostrophic circulation can also be reinterpreted as a source of power generated by the ageostrophic circulation to locally curve the sea surface topography [Eq. (8)]. This interpretation highlights the fundamental dependence of local geostrophic velocities on the global pattern of wind stress, and not just on the local ones. The principle of continuity is key in this diagnostic of energy pathways.

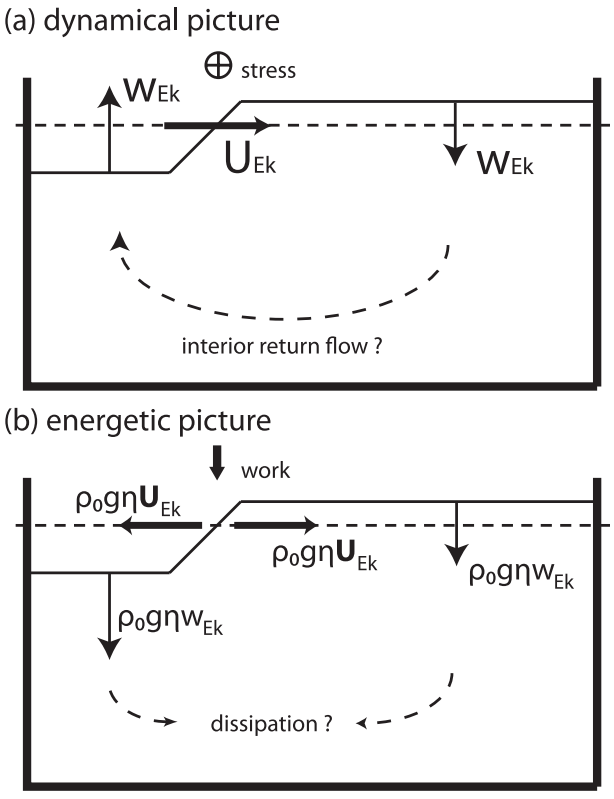

FIG. 6. Schematic description of a wind-driven circulation in a closed basin from (a) a dynamical point of view and (b) an energetic one. These two pictures are equivalent but offer alternative interpretations of how the wind acts on the ocean circulation. Note that the condition of continuity is implicit when considering SSHs relative to the global-mean sea level.

An example of wind-driven circulation is presented in Fig. 6, illustrating the link between dynamical and energetic points of view. In the dynamical point of view, the Ekman transport maintains a deficit of water of one side compared to the other, generating a sea surface slope. This deficit must be compensated by a return flow in the interior, which will depend on processes controlling the stratification and the rate of friction. From the energetic point of view, Ekman pumping works on the hydrostatic pressure field at the surface. Stratification controls the internal pathways of pressure-related energy fluxes until friction dissipates this energy. A complete description of the ocean energetics is still missing, as long as these internal processes are not included.

The description of stratification from an energetic point of view remains particularly challenging, because the effect of buoyancy fluxes must be included, with spatial patterns of surface buoyancy fluxes controlling

in a large part the observed stratification. The question of whether these fluxes are able to power a large-scale circulation in the real ocean is not addressed here. A better description of pressure work sources, sinks, and pathways in the geostrophic interior might provide new insights on this fundamental issue.

Acknowledgments. This work was greatly helped by numerous conversations with Raffaele Ferrari. We also thank Gael Forget, Patrick Heimbach, Jean-Michel Campin, and Matthew Mazloff for their help to carry out diagnostics. This work was supported by the National Ocean Partnership Program (NOPP) through funding of NASA to the ECCO-GODAE Consortium.

APPENDIX A

Kinetic Energy in the Ekman Layer

Consider the kinetic energy balance of a steady-state Ekman layer, where only three forces are acting: Coriolis, the pressure gradient, and the wind stress. The existence of an Ekman depth is assumed, where Ekman circulation and viscous stresses become negligible. The ocean interior is defined as the part below the Ekman depth. A rigid lid approximation is used for simplicity. Variations of density within the Ekman layer are neglected.

Local time-average kinetic energy balance can then be written (e.g., Wunsch and Ferrari 2004),

$$\nabla \cdot (\rho_0 \nu \nabla K_E - p\mathbf{U}) = \rho_0 g w + \rho_0 \varepsilon, \qquad \text{(A1)}$$

where ν is the kinematic viscosity, $K_E = |\mathbf{U}|^2/2$ is the time-mean kinetic energy, $\mathbf{U} = (\mathbf{u}, w)$ is the velocity vector, and p is the hydrostatic pressure (averaging brackets are being suppressed). The two flux terms inside the divergence operator are respectively related to viscosity and pressure terms in the momentum equation. The term $\rho_0 g w$ represents (minus) the conversion of kinetic energy into potential energy, and $\rho_0 \varepsilon$ is the local rate of kinetic energy dissipation.

At the surface, only the viscous term can generate an input of energy, injecting locally the wind stress power input P_τ in the Ekman layer,

$$\begin{aligned}(\rho_0 \nu \nabla K_E)_{z=0} &= [(\rho_0 \nu \partial_z \mathbf{u}) \cdot \mathbf{u}]_{z=0} \\ &= \boldsymbol{\tau}_0 \cdot \mathbf{u}(z = 0) \equiv P_\tau. \end{aligned} \qquad \text{(A2)}$$

At the bottom of the Ekman layer, fluxes of viscous work can safely be neglected, leaving the vertical flux of pressure work $(-pw)_{z=-D}$ as the only means to transfer energy from the Ekman layer to the interior.

Integrating (A1) vertically over the Ekman depth and using the divergence theorem, the balance of kinetic energy in the Ekman layer is obtained,

$$\begin{aligned}P_\tau = (-pw)_{z=-D} &+ \int_{-D}^{0} (p\mathbf{u} - \rho_0 \nu \nabla_h K_E)\, dz \\ &+ \int_{-D}^{0} \rho_0 g w\, dz + \int_{-D}^{0} \rho_0 \varepsilon\, dz. \end{aligned} \qquad \text{(A3)}$$

Here, $z = -D$ is the Ekman depth.

The total wind stress power input P_τ is composed of a geostrophic and an ageostrophic contribution, which are denoted as $P_{\tau,g}$ and $P_{\tau,a}$, respectively. From relation (6), the power input to the geostrophic circulation corresponds to the vertical integral of the work of horizontal pressure forces,

$$\begin{aligned}P_{\tau,g} &\equiv \boldsymbol{\tau}_0 \cdot \mathbf{u}_g(z = 0) = \mathbf{U}_{\mathrm{Ek}} \cdot \nabla_h p_0 \\ &= \int_{-D}^{0} \mathbf{u}_a \cdot \nabla_h p_0\, dz = \int_{-D}^{0} \mathbf{u} \cdot \nabla_h p\, dz, \end{aligned} \qquad \text{(A4)}$$

noting that the horizontal pressure gradient does not vary with depth if density is constant and that the work of horizontal pressure forces on the geostrophic circulation is zero everywhere ($\mathbf{u}_g \cdot \nabla_h p = 0$).

Integrating vertically $\mathbf{U} \cdot \nabla p = \nabla \cdot (p\mathbf{U})$ over the Ekman depth and using the relation (A4), the wind stress work on the geostrophic circulation is found to be either transformed into a pressure work radiating away at the bottom and laterally or converted into potential energy,

$$P_{\tau,g} = (-pw)_{z=-D} + \int_{-D}^{0} \nabla_h \cdot (p\mathbf{u})\, dz + \int_{-D}^{0} \rho_0 g w\, dz. \qquad \text{(A5)}$$

When this relation is integrated spatially over a bounded ocean, the second term on the right vanishes because of the coastal boundary condition, and the last term also vanishes to satisfy the condition of continuity, leaving

$$\iint_{\mathrm{ocean}} P_{\tau,g}\, dS = \int_{\mathrm{ocean}} (-pw)_{z=-D}\, dS, \qquad \text{(A6)}$$

an expression similar to the relation (12), which confirms that the downward flux of pressure work estimated at the surface P_{down} is entirely transmitted below the Ekman layer as a flux of pressure work in our simple Ekman layer model.

In contrast, the wind input to the ageostrophic circulation is entirely used to sustain the Ekman circulation against dissipation in the surface Ekman layer (Wang

and Huang 2004a). This is obtained by subtracting (A5) from (A3) and integrating spatially.

A relation between P_{down} and the flux of pressure work below the Ekman layer is obtained by vertically integrating $\mathbf{U}_g \cdot \nabla_p = \nabla \cdot (p\mathbf{U}_g)$ over the Ekman depth, where $\mathbf{U}_g = (\mathbf{u}_g, w_g)$ is the geostrophic velocity vector,

$$P_{\text{down}} = (-pw)_{z=-D} + \int_{-D}^{0} \nabla_h \cdot (p\mathbf{u}_g)\, dz + \int_{-D}^{0} \rho_0 g w_g\, dz. \quad \text{(A7)}$$

The term P_{down} accounts for all the pressure work terms associated with the geostrophic circulation, including the downward flux of pressure work below the Ekman layer. Thus, P_{down} provides an expression for the rate of pressure work input to the geostrophic interior, which is directly expressed from the surface.

APPENDIX B

Energy Flux Diagnostics at the Equator

Near the equator, geostrophic balance fails. We define a mean vertical Ekman velocity balancing the divergence of transport on both sides of the equator,

$$w_{\text{Ek}}^{\text{equ}} = \frac{\delta \mathbf{U}_{\text{Ek},y}}{L^{\text{equ}}}, \quad \text{(B1)}$$

where $U_{\text{Ek},y}$ is the meridional component of Ekman transport, δ is the difference operator between northern and southern sides of the equator band, and L^{equ} is the width of the equatorial band (taken between $\pm 3°$ of latitude in our diagnostics). This definition preserves the property that the global-mean Ekman pumping velocity is zero.

The local balance between wind-power input with downward and lateral fluxes of pressure work [relation (7)] also breaks down near the equator. Energy fluxes within the equator band are thus estimated indirectly so that the integral relation (12) remains true. This calculation is done by using the divergence on both sides of an equatorial band,

$$P_{\text{down}}^{\text{equ}} = -\rho_0 g \eta^{\text{equ}} w_{\text{Ek}}^{\text{equ}}, \quad \text{(B2)}$$

$$P_{\text{lat}}^{\text{equ}} = \rho_0 g \frac{\delta(\eta \mathbf{U}_{\text{Ek},y})}{L^{\text{equ}}}, \quad \text{and} \quad \text{(B3)}$$

$$P_{\tau,g}^{\text{equ}} = P_{\text{down}}^{\text{equ}} + P_{\text{lat}}^{\text{equ}} = \rho_0 g \frac{\delta[(\eta - \eta^{\text{equ}})\mathbf{U}_{\text{Ek},y}]}{L^{\text{equ}}}, \quad \text{(B4)}$$

where η^{equ} is the latitude-mean sea surface height over the equator band. Although both $P_{\text{down}}^{\text{equ}}$ and $P_{\text{lat}}^{\text{equ}}$ are large, they mostly compensate for each other because η is approximately constant over the equator band at any given longitude.

Ekman pumping volume and energy transports are here defined as longitudinal averages, neglecting zonal transports inside the equatorial band. In reality, the zonal components of transports may be important, but the present method is a suitable first approximation, preserving the global continuity constraints.

The products used in each case are listed: OCCA (Forget 2010) and RH04 are sea surface height products and NCEPbulk (based on a bulk calculation using NCEP winds), Scatterometer Climatology of Ocean Winds (SCOW; Risien and Chelton 2008), NCEP wind stress (Kalnay et al. 1996), and OCCA-adjusted wind stress are wind stress products. More details can be found in the core text and in appendix C.

APPENDIX C

Comparison of Products

Several wind stress and sea surface height products are here used to assess the robustness of spatial patterns of wind-power inputs described in the main text. All products were reinterpolated onto the OCCA grid with a 1° horizontal resolution before calculating energy fluxes. This approach permits use of the same discretization procedure for all calculations. Discretization error is always a minor contribution, and so it can be safely neglected.

The sensitivity of energy diagnostics to wind stress is tested using two different wind stress products apart from NCEPbulk. The first product is derived from the Scatterometer Climatology of Ocean Winds (SCOW) of Risien and Chelton (2008), derived from an 8-yr record of satellite [Quick Scatterometer (QuikSCAT)] wind stress measurements. Because scatterometers measure directly the surface wind stress, the relative wind effect should be implicitly taken into account in this product. Comparisons with ship-based observations show RMS differences on the order of 0.01 N m^{-2} in tropical and subtropical areas, increasing rapidly to more than 0.05 N m^{-2} in subpolar areas (Risien and Chelton 2008). However, these comparisons must be considered with caution, because ship-based observations remain sparse in subpolar regions. The second product, called NCEP, is the mean NCEP–NCAR wind stress field (Kalnay et al. 1996). A comparison of zonal-mean wind stress profiles, both zonal and meridional, appears in Fig. C1. SCOW and NCEPbulk zonal wind stress are

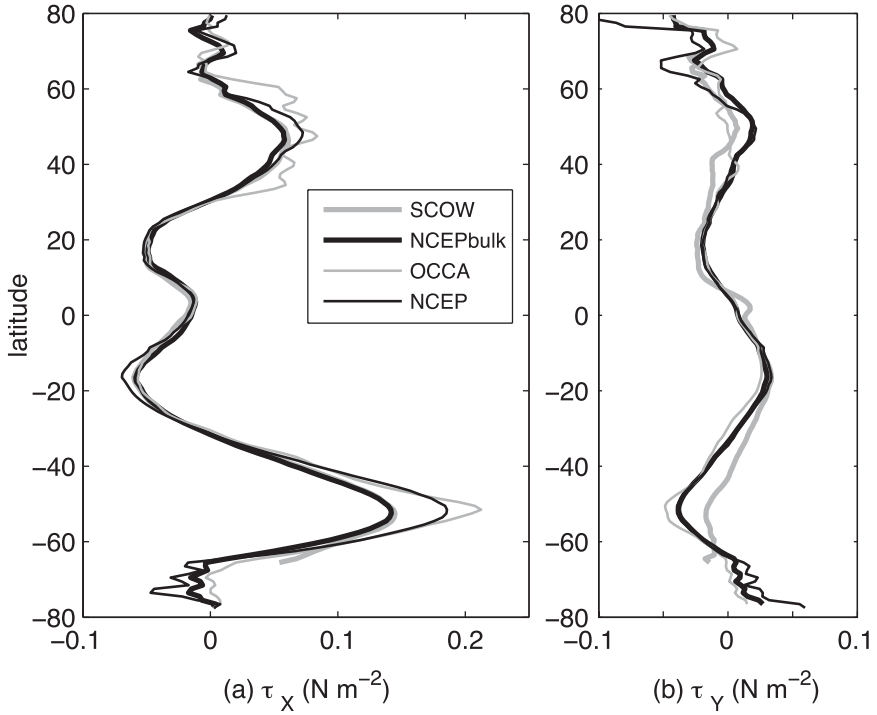

FIG. C1. Comparison of zonal-mean wind stress products for (a) zonal and (b) meridional components. The wind stress products are NCEPbulk (based on a bulk calculation using NCEP winds), SCOW (Risien and Chelton 2008), NCEP wind stress (Kalnay et al. 1996), and OCCA-adjusted wind stress (Forget 2010). More details can be found in section 3a and in appendix C.

similar everywhere. NCEP zonal wind stress is stronger than SCOW and NCEPbulk in subpolar areas, especially in the ACC band, where the maximum zonal wind stress is stronger by 25%. SCOW meridional wind stress is weaker than both NCEP and NCEPbulk. These inconsistencies represent one of the very few measures of uncertainties in oceanic wind stress estimates.

Calculations using SCOW and NCEPbulk wind stress products are similar, but NCEP-based estimates are 20% larger, mainly because of the larger zonal wind stress in the ACC band. Our total power input estimates agree with similar estimates in the literature. From daily QuikSCAT wind stresses combined with altimetric sea surface height, a combination similar to RH04–SCOW, Hughes and Wilson (2008) estimated a power total of 760 GW with 480 GW in the Southern Ocean and Scott and Xu (2009) also found 760 GW of power input in the extratropics. Using the NCEP wind stress field, Huang et al. (2006) obtained 840 GW and Scott and Xu (2009) found 940 GW, in agreement with our RH04–NCEP estimate. Scott and Xu (2009) proposed a 100-GW estimate for the direct wind work in the tropical band, much higher than the values found here (generally lower than 10 GW), but it is not clear to us how they obtained their estimate.

Qualitative comparisons of the spatial patterns of pressure work inputs shows generally a good agreement with the reference solution presented in Fig. 3b (see Figs. C2a–c). The main difference is seen with OCCA–SCOW (Fig. C2a), where P_{down} is artificially forced to large values along the sea ice edge because of the absence of wind stress data in ice-covered areas.

The sensitivity of energy diagnostics to the sea surface height product is also tested with the mean sea surface height derived from RH04. This product results from the combination of satellite data (gravimetry and altimetry) with in situ data (drifting floats and hydrography). Because the RMS difference with OCCA is 7 cm out of a total range of about 2 m, it is not surprising to find a small sensitivity to the choice of sea surface height product for any given wind stress product (see Table 1), with differences around 5% of the total input.

Larger spatial discrepancies are seen when the OCCA-adjusted wind stress field is used for the calculation (see Fig. C2d). OCCA is initially forced by NCEP–NCAR winds, using the bulk formulation of Large and Yeager (2004). The NCEP–NCAR wind field is then adjusted during the model minus observation minimization process. Final OCCA wind stress field is thus a modified

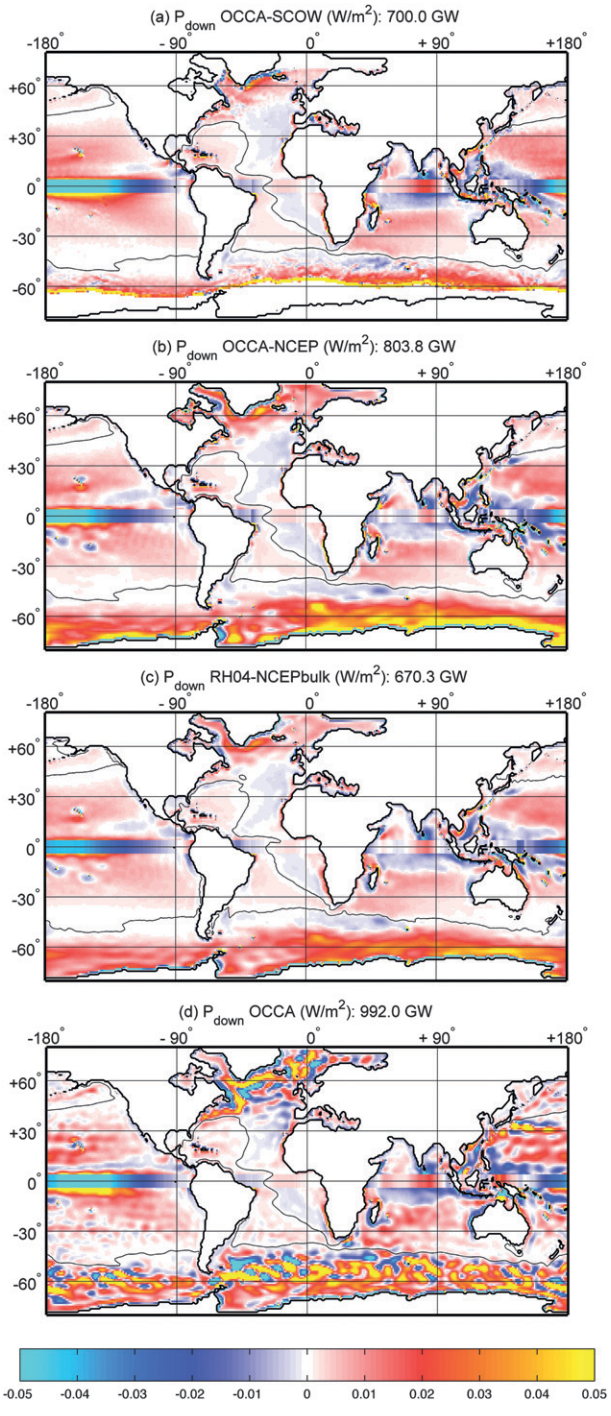

FIG. C2. Time-mean contribution of P_{down} estimated using different combinations of wind stress and SSH products. Two mean SSH products are used: OCCA (Forget 2010) and RH04. Wind stress products are as in Fig. 7.

version of NCEPbulk. The OCCA wind stress field departs importantly from NCEPbulk, having in particular zonal wind stress within the ACC band increased by 50% (see Fig. C1). It is not surprising that the total power input increases by 50% compared to OCCA–NCEPbulk (Table 1).

Not only the total power input is increased by OCCA wind adjustments, but the spatial pattern becomes also more patchy, with the presence of strong negative–positive pressure work spatial anomalies that are generally not seen in the OCCA–NCEPbulk field (see Fig. 3b). These wind adjustments are reshaping the pressure field at small scale, possibly compensating for some missing physics in the model. We suspect a misrepresentation of finescale current topography interaction at the OCCA resolution as a principal source of bias counterbalanced by wind adjustments. A more detailed study is still required to assess the detailed impact of OCCA wind adjustments, including a study of changes in the time-varying contribution.

REFERENCES

Duhaut, T. H. A., and D. N. Straub, 2006: Wind stress dependence on ocean surface velocity: Implications for mechanical energy input to ocean circulation. *J. Phys. Oceanogr.,* **36,** 202–211.

Fofonoff, N. P., 1981: The Gulf Stream system. *Evolution of Physical Oceanography: Scientific Surveys in Honor of Henry Stommel,* B. A. Warren and C. Wunsch, Eds., MIT Press, 112–139.

Forget, G., 2010: Mapping ocean observations in a dynamical framework: A 2004–06 ocean atlas. *J. Phys. Oceanogr.,* **40,** 1201–1221.

Gill, A. E., J. S. A. Green, and A. J. Simmons, 1974: Energy partition in the large-scale ocean circulation and the production of mid-ocean eddies. *Deep-Sea Res. I,* **21,** 499–528.

Huang, R. X., W. Wang, and L. L. Liu, 2006: Decadal variability of wind-energy input to the world ocean. *Deep-Sea Res. II,* **53,** 31–41.

Hughes, C. W., and C. Wilson, 2008: Wind work on the geostrophic ocean circulation: An observational study of the effect of small scales in the wind stress. *J. Geophys. Res.,* **113,** C02016, doi:10.1029/2007JC004371.

Kalnay, E., and Coauthors, 1996: The NCEP/NCAR 40-Year Reanalysis Project. *Bull. Amer. Meteor. Soc.,* **77,** 437–471.

Large, W., and S. Yeager, 2004: Diurnal to decadal global forcing for ocean and sea-ice models: The data sets and flux climatologies. NCAR Tech. Note NCAR/TN-460+STR, 112 pp.

Marshall, J., A. Adcroft, C. Hill, L. Perelman, and C. Heisey, 1997: A finite-volume, incompressible Navier-Stokes model for studies of the ocean on parallel computers. *J. Geophys. Res.,* **102** (C3), 5753–5766.

Mazloff, M. R., P. Heimbach, and C. Wunsch, 2010: An eddy-permitting Southern Ocean state estimate. *J. Phys. Oceanogr.,* **40,** 880–899.

Orsi, A. H., T. Whitworth III, and W. J. Nowlin, 1995: On the meridional extent and fronts of the Antarctic Circumpolar Current. *Deep-Sea Res. I,* **42,** 641–673.

Pedlosky, J., 1968: An overlooked aspect of the wind-driven oceanic circulation. *J. Fluid Mech.,* **32,** 809–821.

Rio, M.-H., and F. Hernandez, 2004: A mean dynamic topography computed over the world ocean from altimetry, in situ measurements, and a geoid model. *J. Geophys. Res.,* **109,** C12032, doi:10.1029/2003JC002226.

Risien, C. M., and D. B. Chelton, 2008: A global climatology of surface wind and wind stress fields from eight years of QuikSCAT scatterometer data. *J. Phys. Oceanogr.,* **38,** 2379–2412.

Scott, R. B., and Y. Xu, 2009: An update on the wind power input to the surface geostrophic flow of the world ocean. *Deep-Sea Res. I,* **56,** 295–304.

Stern, M. E., 1975: *Ocean Circulation Physics*. Academic Press, 246 pp.

Stommel, H., 1957: A survey of ocean current theory. *Deep-Sea Res. I,* **4,** 149–184.

von Storch, J.-S., H. Sasaki, and J. Marotzke, 2007: Wind-generated power input to the deep ocean: An estimate using a 1/10 general circulation model. *J. Phys. Oceanogr.,* **37,** 657–672.

Wang, W., and R. X. Huang, 2004a: Wind energy input to the Ekman layer. *J. Phys. Oceanogr.,* **34,** 1267–1275.

——, and ——, 2004b: Wind energy input to the surface waves. *J. Phys. Oceanogr.,* **34,** 1276–1280.

Wunsch, C., 1998: The work done by the wind on the oceanic general circulation. *J. Phys. Oceanogr.,* **28,** 2332–2340.

——, and R. Ferrari, 2004: Vertical mixing energy and the general circulation of the oceans. *Annu. Rev. Fluid Mech.,* **36,** 281–314.